A Surface-Potential Based Sub-Circuit Model of I-V Characteristics In AlGaN/GaN HEMTs

Nebojša Janković, Soroush Faramehr and Petar Igić

Abstract - In this paper, the surface-potential based sub-circuit model of AlGaN/GaN HEMT yielding accurate and continuous I-V characteristics in the whole operation range is described. The model includes some important physical phenomena affecting device DC operation like 2DEG charge quantization, electron velocity saturation, high-field mobility degradation, channel length modulation, polarization charge and self-heating effects. A good fit between the sub-circuit model and the experimental I-V characteristics of Al0.25Ga 0.75N/GaN HEMT is demonstrated with SPICE simulations.

Keywords-Surface-Potential,Sub-Circuit Model, AlGaN/GaN, HEMTs

I. INTRODUCTION

AlGaN/GaN high electron mobility transistors (HEMTs) are considered as the best candidate for high-speed, microwave and high-power applications due to III-Nitride material properties such as high electron mobility, wide band-gap and large polarization charge enabling high current densities [1]. With significant progress in the improvements of AlGaN/GaN structure quality and performance of GaN HEMTs, the exploitation of full potential of these devices requires the advanced electrical models for circuit simulations. Among various compact models [2,3], the surface-potential-based (SP) models of GaN HEMTs appears advantageous because of the mostly physics-based model parameters and the ability to precisely describe the I-V characteristics in the whole operation range. In addition, the SP models have been proven very successful in the past for modeling advanced MOSFETs [4,5,6].

The majority of compact SP models of GaN HEMTs proposed so far [7-15] are based on deriving the approximate analytical expressions either for the electrostatic potential ψ_s of quantum-well-formed channel [7-11,13,14] and/or the mobile charge density n_s of two-dimensional electron gas (2-DEG) [8,9,12]. The analytical relations for ψ_s and/or n_s are subsequently used in drift-diffusion continuity equation with certain carrier transport models for obtaining the I-V characteristics of GaN HEMTs [8-15]. The main difficulty in deriving the analytical expressions of ψ_s and/or n_s stems from their complicated variations with the applied gate-source V_{GS} and drain-source V_{DS} voltages. simplifying the Schrodinger's and/or Poisson's equations in different Consequently, all SP-based compact models [7-15] are essentially developed by regions of device operation and using the suitable chosen smoothing functions to cover the whole V_{GS} and V_{DS} ranges.

In this paper, the SP-based sub-circuit (SPSC) model of AlGaN/GaN HEMT capable to accurately produce continuous I-V characteristics in the whole device operational range is presented and implemented in SPICE [23]. It avoids the need for the derivation of complex analytical expressions in compact modeling and allows for easy inclusion of some important physical phenomena such as 2DEG charge quantization, electron velocity saturation, high-field mobility degradation, channel length modulation, polarization charge and self-heating effects. A good fit of the SPSC model with experimental I-V characteristics of Al0.25Ga 0.75N/GaN HEMT is demonstrated in this work using SPICE simulations.

II. MODEL DESCRIPTION

Fig.1.a and Fig.1.b show the cross section of AlGaN/GaN HEMT and the schematics of the corresponding SPSC model, respectively.

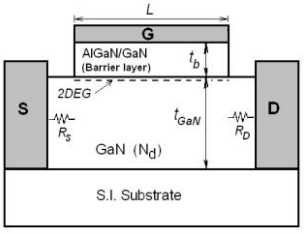

Fig. 1.a

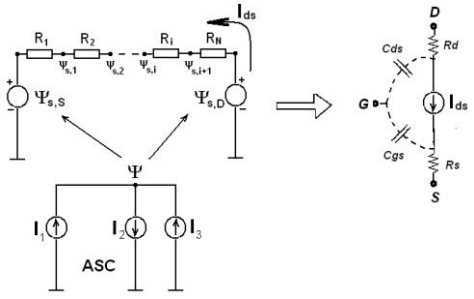

Fig. 1.b

Fig. 1. a) The AlGaN/GaN HEMT cross section with relevant parameters. b) The schematics of SPSC model with ASC

Nebojsa Jankovic: Faculty of Electronic Engineering Nis, University of Nis, Aleksandra Medvedeva 14, Nis, Serbia; e-mail: nebojsa.jankovic@elfak.ni.ac.rs
Soroush Faramehr, and Petar Igić: Electronic Systems Design Centre (ESDC), College of Engineering, Swansea University, Swansea SA1 8EN,UK.

Some important device structural parameters depicted in Fig.1.a include a gate length of L, a gate barrier of thickness t_b, a hetero-interface 2DEG sheet charge, an unintentionally doped GaN layer of thickness tGaN of doping N_d sitting on a semiinsulating (S.I.) substrate, and source and drain contact regions with parasitic resistances RS and RD. The channel-equivalent circuit is the core of the SPSC model as shown in Fig.1.b. It consists of N identical segmental channel resistors Ri (i=1,N) whose non-linear resistivity are the function of local node surface potentials $\psi_{s,i}$. The two voltage generators $\psi_{s,S}$ and $\psi_{s,D}$ shown in Fig.1.b denote the boundary surface potentials at the source and the drain ends of the channel, respectively, determined by the gate, source and drain biasing voltages V_S, V_{GS} and V_{DS}, respectively. The drain current I_{DS} is obtained from solving the channel equivalent sub-circuit with SPICE simulations. It can be copied via an ideal current source into the main sub-circuit model with necessary added AC or other parasitic external elements (resistance, capacitances and/or inductances) [14] for forming the final large-signal GaN HEMT as illustrated also in Fig.1.b.

2.1 Extracting the channel boundary potentials

Recently, Jana et al. [13] have derived the implicit surface potential equation used for calculating the channel surface potential ψ_s of AlGaN/GaN HEMTs with explicit appearance of the polarization charge σ_π. It was obtained from solving the Poisson's equation with charge sheet approximation and Boltzmann electron distribution function [16].

$$\frac{1}{2}\left(\frac{V_{gp}-\Psi_s}{t_b}\right)^2+\frac{q\sigma_\pi}{\varepsilon_s}\left(\frac{V_{gp}-\Psi_s}{t_b}\right)+\frac{q}{\varepsilon_s}\left[\begin{array}{l}\Psi_s N_d+\vartheta_t p_0\left(1-e^{-\frac{\Psi_s}{\vartheta_t}}\right)\\ -\vartheta_t N_d e^{-\frac{V_x}{\vartheta_t}}\left(e^{-\frac{\Psi_s}{\vartheta_t}}-1\right)\end{array}\right]=0 \quad (1)$$

where $V_{gp}=V_{GS}-V_p$ is the effective gate voltage, V_p is the channel cut-off voltage and V_x is the local channel potential under the influence of drain voltage V_{DS}. The meanings of other related symbols appearing in (1) are shown in Table I. The boundary surface potentials $\psi_{s,S}$ and $\psi_{s,D}$ are obtained in the SPSC model from SPICE simulations of the auxiliary sub-circuit (ASC) that is also shown in Fig.1.b. It consists of three non-linear voltage controlled current sources I_1, I_2 and I_3 expressed with respect to a voltage variable ψ_s as :

$$I_1=\frac{q}{\varepsilon_s}\vartheta_t N_d e^{-\frac{V_x}{\vartheta_t}}\left(e^{\frac{\Psi_s}{\vartheta_t}}-1\right),$$

$$I_2=\frac{q}{\varepsilon_s}\vartheta_t p_0\left(e^{-\frac{\Psi_s}{\vartheta_t}}-1\right), \quad (2)$$

$$I_3=\frac{1}{2}\left(\frac{V_{gp}-\Psi_s}{t_b}\right)^2+\frac{q\sigma_\pi}{\varepsilon_s}\left(\frac{V_{gp}-\Psi_s}{t_b}\right)+\frac{q}{\varepsilon_s}\Psi_s N_d$$

The functional expressions of I_1, I_2 and I_3 in (1) are obtained after re-grouping the additive terms of the implicit closed form equation (1). The two identical ASC are necessary to use in the SPSC model of Fig.1 for obtaining $\psi_{s,S}$ and $\psi_{s,D}$, with $V_x=V_S$ and $V_x=V_{DS}$ replaced in (1) for the source and the drain potential at the channel ends, respectively. The node potential ψ depicted in ASC of Fig.1 represents the solution of the surface potential equation, since the Kirkhoff's zero net current condition equality $I_1-I_2+I_3=0$ actually recovers the original equation (1).

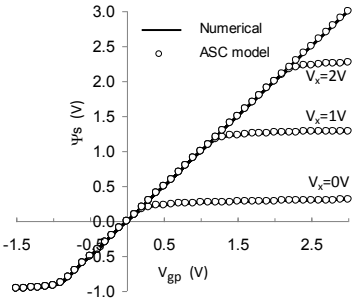

Fig. 2. Surface potential ψ_s as a function of the effective gate voltage V_{gp} for different local channel potentials V_x obtained with SPICE simulation of ASC and from numerically solving the original implicate equation [13].

Fig.2 shows an excellent agreement between ψ_s versus V_{gp} dependences obtained for different local channel potentials V_x with SPICE simulations of ASC and from numerically solving the implicate equation (1). The full overlap between the numerical and SPICE simulated curves as shown in Fig.2 validates the efficiency of ASC for extracting $\psi_{s,S}$ and $\psi_{s,D}$ in the SPSC model.

2.2 Modeling the 2DEG charge density n_s

The quantum-mechanical effects are not considered in deriving the original channel potential equation (1) for the sake of derivation simplicity [13]. In addition, the quantum corrections of 2DEG well potential has a minor effect on the output characteristics of AlGaN/GaN HEMTs due to

pre-dominance of polarization charge σ_π [17]. However, the quantization of 2DEG charge density n_s is useful to include in the SP -based HEMT models since it improves the overall device modeling accuracy [9,10,11,12]. A few complex analytical expressions of n_s with charge quantization have been reported recently [9,10,12,19] employing various interpolation functions between different regions of device operation. In contrast, a simple analytical relation between n_s and ψ_s is derived in this work and employed in the SPSC model that avoid possible convergence problems in SPICE simulations. Based on the compact analytical relation for 2DEG charge density at hetero-interface [18], an approximate implicit equation for calculating n_s is developed as shown in the Appendix (eq. A.5). It is repeated here as:

$$V_{gp} - \psi_s - \gamma_0 n_s^{\frac{2}{3}} - \frac{t_b q}{\varepsilon_{GaN}} n_s = \vartheta_t \ln\left(e^{-\frac{n_s}{D\vartheta_t}} - 1 \right) \quad (3)$$

where the meaning of physical parameters q, D, γ_0, ε and υ_t are listed in Table I.

The new implicit equation (3) shows that n_s is a complex function of V_{gp} and V_x due to a voltage dependence of ψ_s as can be observed in Fig.2. The values of ψ_s obtained for different V_{gp} and V_x from SPICE simulations of ASC as for Fig.2 are also used for numerically solving (3) over the variable n_s.

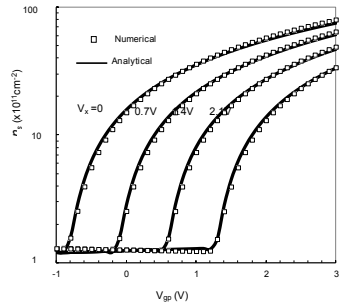

Fig. 3.a

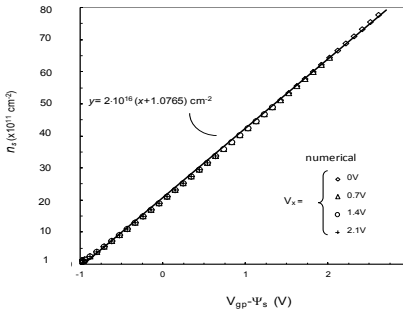

Fig. 3.b

Fig. 3. a) Comparison of the numerical calculations and the linear analytical model (Fig.3.b) of n_s versus the gate effective voltage V_{gp} for different local channel potentials V_x. b) A unique linear dependence of n_s versus the effective channel surface potential (V_{gp}-ψ_s) regardless of different local channel potential V_x.

Fig.3.a shows a non-linear behavior of n_s with V_{gp} obtained from numerically solving (3) for different constant values of V_x. However, when re-plotting the same numerical $n_s(V_{gp})$ curves from Fig.3.a, but now against the voltage difference (V_{gp}-ψ_s) on the x-axes, a unique linear dependence of n_s is obtained regardless of V_x as shown in Fig.3.b. It can be well approximated with the function $n_s = 2 \times 10^{12} (V_{gp} - \psi_s + 1.0765)$ cm $^{-2}$ depicted by solid line in Fig.3.b. The accuracy of the later linear approximation can be additionally validate with the results in Fig.3.a showing an excellent agreement between the numerical and the analytical values of n_s obtained with linear approximation from Fig.3.b. Following these results, the charge density $n_{s,I}$ of the i-th segment of the SPSC model can now be expressed as:

$$n_{s,i} = a\left(V_{gp} - \psi_{sm}\right) + b, \quad (4)$$

where a and b become new model fitting parameters. The mid-potential $\psi_{sm}=(\psi_{s,i}+\psi_{s,i-1})/2$ of the i-th segment is employed in (4) in order to improve the simulation accuracy of SPSC model.

2.3 Expressing the segmental resistance R_i

Using the charge-sheet approximation [16], the channel segmental resistance R_i appearing in Fig.1 can be analytically expressed as:

$$R_i = \frac{w_i}{W q \mu_n n_{s,i}} \quad (5)$$

where μ_n is the channel carrier's mobility, $w_i = L/N$ is the resistor length, L is the gate length, W is the channel width and q is the electron charge. The longitudinal and vertical electric filed dependences of the electron mobility in 2DEG are modeled in (4) by the following approximate expressions [10]:

$$\mu_n\left(E_x\right) = \frac{\mu_{LF} E_x}{1 + \dfrac{u_a \left| E_x \right|}{E_T}}, \qquad \mu_{LF}\left(E_{y.eff}\right) = \frac{\mu_0}{1 + p_1 \left| E_{y.eff} \right| + p_2 E_{y.eff}^{\,2}}, \quad (6)$$

where μ_{LF} is the low longitudinal field mobility, μ_0 is the low vertical field mobility, E_x is the longitudinal electric field along the channel, E_T is the critical electric field, $E_{y,\mathrm{eff}}$

denotes the effective vertical field in the GaN layer, and u_a p_1, p_2 are the fitting parameters. The mobility formulas (6) holds for relatively low values of V_{DS} e.g as long as $E_x < E_T$. Following the average-potential approximation [9, 10], the electric fields E_x and $E_{y,\text{eff}}$ are easily expressed in the SPSC model as:

$$E_x = \frac{\psi_i + \psi_{i-1}}{w_i}, \tag{7}$$

$$E_{y,eff} = \varepsilon_s \frac{V_{gp} - \frac{\psi_{s,S} + \psi_{s,D}}{2}}{d\varepsilon_{GaN}}, \tag{8}$$

where ε, t_b and ε_{GaN} are physical parameters with meanings listed in Table I.

Finally, for obtaining realistic I-V characteristics that reasonably agree with measured output curves of fabricated GaN HEMTs, the channel length modulation (CLM) phenomena and the self-heating effects (SHE) must be taken into account since they largely influence the device output current I_{DS}. These important physical effects are included in the SPSC model with semi-empirical relations modifying (4) as:

$$R_i = \frac{w_i\left(1 - \lambda V_{DS}^m\right)}{Wq\mu_n n_{s,i}}\left(1 + \beta \cdot \left|V_{gp} V_{DS}\right|\right). \tag{9}$$

The CLM phenomena is expressed in (9) with simple term $(1 - \lambda \cdot V_{DS}^m)$ modulating w_i,where λ and m are fitting parameters [6]. The SHE is also included in (9) by adding a new multiplicative term $(1+\beta \cdot |V_{gp} \cdot V_{DS}|)$, with β as fitting parameter. The latter effectively increases R_i at higher V_{gp} and/or V_{DS} causing the decrease of I_{DS} when the device operates at higher power level. A highly simplified SHE model implemented in (9) is based on the assumption that SHE are dominantly expressed as degradation of the mobility of 2DEG electrons owning to a local increase of channel temperature [20]. Note that a drain-induced barrier lowering (DIBL) effect important for highly-scaled GaN HEMTs, is not considered in this work since the referent experimental device was with relatively long gate (L=1μm). However, the DIBL effect can be easily included in the SPSC model with any suitable analytical expression describing the shift of channel cut-off voltage V_p with V_{DS} and/or L [25].

III. Results and Discussion

Fig.4.a and Fig.4.b compares the simulated I_{DS}-V_{DS} and I_{DS}-V_{GS} characteristics of conventional $Al_{0.25}Ga_{0.75}N$/GaN HEMT against the experimental DC measurements [26]. The numerical values of all model parameters used in SPICE simulations are shown in Table I. A fairly good matching between simulated and measured [26] characteristics is observed in Fig.4 in spite of using a highly simplified expressions for CLM and SHE effects in the SPSC model. To further improve modelling accuracy, the influence of access regions parasitic resistances (Fig.1.a) is included in SPICE simulations by adding two fixed resistors R_s and R_d in the external circuit as shown in Fig.1.b.

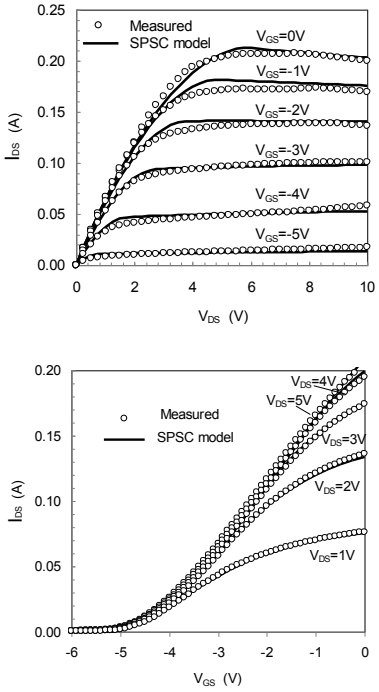

Fig. 4. Compares of the modelled: (a) I_{DS}-V_{DS} and (b) I_{DS}-V_{GS} characteristics with experimental data of $Al_{0.25}Ga_{0.75}N$/GaN HEMT with $L=1\mu m$ [26]

The Gummel symmetry test [24] is also performed to validate the correctness of the SPSC model with respect to drain/source symmetry. A voltage source V_m is applied at the drain terminal, whereas $-V_m$ is applied at the source terminal. V_m is varied from −1 to 1 V . Fig.5 shows the first derivative of I_{DS} versus V_m extracted for various V_{GS} from SPICE simulations. The results in Fig. 4 shows that the SPSC model passes the basic test condition of the symmetrical and continuous first derivative of I_{DS} with respect to V_m and at V_m=0, respectively [24].

Fig. 6 shows the dependence of relative numerical error of I_{DS} and g_m versus the number of channel segments N used in simulations with the SPSC model. The relative error is defined here as the difference between the values of I_{DS} and g_m obtained for N <10 against those simulated with N=10, e.g. rel.err.=$(I_{DS|\,N<10} - I_{DS|\,N=10})/I_{DS|\,N=10}$x100%.

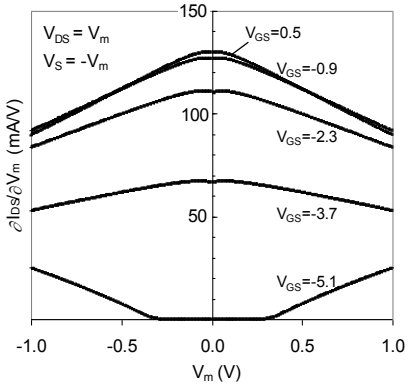

Fig. 5. Gummel symmetry characteristics of the SPSC model simulated for different V_{GS} and V_m= -1 to 1V, 0.01V steps, $V_{DS} = V_m$ and $V_{DS} = V_m$

In the example of GaN HEMT with L=1um, Fig.6 shows that only N=6 is sufficient to use in the SPSC model for achieving the relative numerical error smaller than 1%.

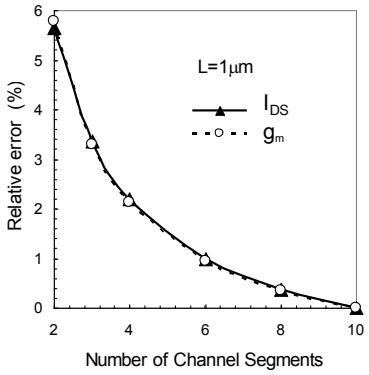

Fig. 6

Fig. 6. Relative numerical error of I_{DS} and g_m versus the number of channel segments N used in SPICE simulations with the SPSC model.

A steep decrease of relative error of I_{DS} and/or g_m with increasing N, which is observed in Fig.6, also indicates the high efficiency of SPSC model with respect to fast numerical converging and short CPU time required in SPICE simulation.

IV. Conclusions

In this paper, the surface-potential-based sub-circuit (SPSC) model of AlGaN/GaN HEMT yielding continuous I-V characteristics in the whole operational range is described and implemented in SPICE. It allows for easy inclusion of important physical phenomena such as electron velocity saturation, high-field mobility degradation, channel length modulation and self-heating effects and avoids the need for the derivation of complex analytical expressions in compact modeling. A good fit of the SPSC model with experimental I-V characteristics of $Al_{0.25}Ga_{0.75}N$/GaN HEMT is demonstrated with SPICE simulations.

TABLE I
PARAMETERS USED IN SPICE SIMULATION

Simbol	Description	Value
L	Gate length	1μm
W	Gate width	400 μm
N	Number of segments	10
V_{off}	Cut-off voltage	-5.9V
R_S	Source contact resistance	0.45 Ω
R_D	Drain contact resistance	1 Ω
t_b	Thickness of the gate barrier layer	33nm
σ_π	Polarization sheet charge at the heterointerface	$1e^{17}$ m^{-2}
n_i	Intrinsic carrier concentration	$2.9e^{-4}$ m^{-3}
N_d	Doping of unintentional doped GaN	$1e^{22}$ m^{-3}
D	Density of states at the conduction band edge	$1.001e^{18}cm^{-3}$
q	Electron charge	$1.609e^{-19}$ C
υ_t	Thermal voltage	0.0259 V
ε_s	Permitivity of AlGaN barrier layer	$7.965e^{-11}$
ε_{GaN}	Permitivity of GaN layer	7.88 e^{-11}
E_T	Critical electric field	1.68 e^7 V/m
γ_0	Experimentally determined parameter	$2.12e^{12}$ $m^{4/3}$
a, b	Fitting parameters of the n_s model	$2e^{16}$ $V^{-1}cm^{-2}$, $2.135e^{16}$ $V^{-1}cm^{-2}$
λ , m	SCE model parameters	0.105 V^{-1}, 0.5
β	SHE model parameter	9.4e-3
μ0	Low field mobility	$3.2e^{-2}m^2V^{-1}s$
u_a , p_1, p_2	Mobility degradation parameters	2.1, $7e^{-9}$ mV^{-1} $3.9e^{-17}m^2V^{-2}$
p_0	n_i^2/N_d, The equilibrium hole charge of GaN	
n_s	The density of the 2DEG	
E_f	Position of Fermi level	
E_0	Position of first energy level	
μ_0	Low vertical field mobility	
$E_{y,eff}$	Effective vertical electric field	
E_x	Longitudinal electric field	

V. APENDIX I

Here the derivation of (2) is explained in more detail. Based on the self consistent solution of Schrodinger's and Poisson's equations in the wide band-gap semiconductor, the analytical relation of 2DEG charge density for HEMTs has been derived using the triangular quantum well approximation and considering only the two lowest subband energy levels E_1 and E_0 [18,22]. Since at the AlGaN/GaN hetero-interface, the upper energy level E_1 is larger than the Fermi energy E_f for the complete range of V_{GS} and because E_1 is significantly larger than E_0 over the same range ($E_1 \approx 3E_0$), the electron contributed by E_1 and higher energy band to n_s can be safely ignored [10,12]. Then, the analytical expression for 2DEG charge density [18,22] can be simplified as:

$$n_s = Dv_{th}\left[\ln\left(e^{\frac{E_f - E_0}{v_{th}}} + 1\right)\right] \tag{A.1}$$

where D is the 2DEG density of states. The dependence of lowest energy sub-band E_0 versus n_s is approximated by [21]:

$$E_0 = \gamma_0 n_s^{\frac{2}{3}} \tag{A.2}$$

where γ_0 is the experimentally determined parameter with value shown in Tab I. Assuming that the AlGaN layer is completely ionized, the following relation exists:

$$n_s = \frac{\varepsilon_{GaN}}{qt_b}\left(V_{gp} - \psi_s - E_f\right) \tag{A.3}$$

From (A.3) , E_f is expressed as.

$$E_f = \frac{qt_b}{\varepsilon_{GaN}} n_s - V_{gp} + \psi_s \tag{A.4}$$

Replacing E_0 and E_f from (A.2) and (A.4) into (A.1), the implicit equation for calculating n_s with ψ_s as variable is obtained as:

$$V_{gp} - \psi_s - \gamma_0 n_s^{\frac{2}{3}} - \frac{qt_b}{\varepsilon_{GaN}} n_s = \vartheta t \ln\left(e - \frac{n_s}{D\vartheta t} - 1\right) \tag{A.5}$$

REFERENCES

[1] Johnson, W., Piner, E.L., *"GaN HEMT Technology in GaN and ZnO-Based Materials and Devices"*, edited by Pearton, S.J., Springer, Heidelberg, 2012, pp. 209-238.

[2] Chen, Q., "*Latest advances in gallium nitride HEMT modeling*", 12th IEEE International Conference on Solid-State and Integrated Circuit Technology (ISCIST), 2014, pp: 1-4.

[3] Shanthi, J., Vimala, P., Shanthi, J. Vimala, P, "*High Electron Mobility Transistor: A Review on Analytical Models*", International Journal for Innovative Research in Science & Technology (IJIRST), Vol. 3, 2016, pp: 103-114.

[4] Paydavosi N., Venugopalan S., Chauhan Y.S., Duarte J.P., Jandhyala S., Niknejad A.M., Hu C.C., "*BSIM-SPICE Models Enable FinFET and UTB IC designs*", *IEEE Access*, vol. 1, pp. 201–215, 2013.

[5] Jankovic N., Pesic T., "*Non-quasi-static physics-based circuit model of fully-depleted double-gate SOI MOSFET*", Solid-State Electronics, Vol. 49, 2005, pp: 1086-1089.

[6] Pesic T., Jankovic N., "*A Compact Non-Quasi-Static MOSFET Model based on the Equivalent Non-Linear Transmission Line*", IEEE Trans. Computer-Aided-Design Integrated Circ. Systems, Vol. 27, 2005, pp: 1550-1561.

[7] Khandelwal S., Chauhan Y.S., Fjeldly T.A., "*Analytical Modeling of Surface-Potential and Intrinsic Charges in AlGaN/GaN HEMT Devices*", IEEE Trans. Electron Devices, Vol. 59, 2012, pp: 2856–2860.

[8] Khandelwal S., Fjeldly T.A., "*A surface-potential-based drain current model for study of non-linearities in AlGaAs/GaAs HEMTs*", in Proc.Compound Semicond. IC Symp., 2012, pp: 1-4.

[9] Khandelwal S., Fjeldly T.A., "*A physics based compact model of I–V and C–V characteristics in AlGaN/GaN HEMT devices*", Solid-State Electronics, Vol. 76, 2012, pp: 60-66.

[10] Cheng, X.,Wang, Y., "*A surface-potential-based compact model for AlGaN/GaN MODFETs*", IEEE Transactions on Electron Devices, Vol. 58, 2011, pp: 448-454.

[11] Patrick M., Hahe R. HSP, "*A surface-potential-based compact model of AlGaN/GaN HEMTs power transistors*", 10th MOS-AK/GSA ESSDERC/ESSCIRC Workshop Bordeaux, 2011.

[12] Khandelwal S., Goyal, N., Fjeldly T.A., "*A physics-based analytical model for 2DEG charge density in AlGaN/GaN HEMT devices*", IEEE Transactions on Electron Devices, Vol. 58, 2011, pp: 3622-3625.

[13] Jana R., Jena D., "*A surface-potential based compact model for GaN HEMTs incorporating polarization charges*", IEEE 70th Annual Device Research Conference, 2012, pp: 147-148.

[14] Jun, L., Zhiping, Y., Lingling, S., "*A complete and accurate surface-potential based large-signal model for compound semiconductor HEMTs*", Journal of Semiconductors, Vol. 35, 2014.

[15] Khandelwal, S., Yadav, C., Agnihotri, S., Chauhan, Y.S., Curutchet, A., Zimmer, T., Jean- Jaeger D.C.,

Defrance N., Fjeldly, T.A., "*A. Robust surface-potential-based compact model for GaN HEMT IC design*", IEEE Transactions on Electron Devices, Vol. 60, 2013, pp: 3216-3222.

[16] Brews J. R., "*A charge-sheet model of the MOSFET*", Solid-State Electronics, Vol. 21, 1978, pp: 345–355.

[17] Yamakawa S., Goodnick S., Aboud S., Saraniti M., "*Quantum corrected full-band cellular Monte Carlo simulation of AlGaN/GaN HEMTs*", J. Comput. Electron, Vol. 3, 2004, pp: 299–303.

[18] Lee K., Shur M.S., Drummond T.J., Morkoc H., "*Electron density of the two dimensional electron gas in modulation doped layers*", J.Appl. Phys, Vol. 54, 1983, pp: 2093–2096.

[19] Pu J., Sun J., Zhang D., "*An accurate polynomial-based analytical charge control model for AlGaN/GaN HEMT*", Semiconductors, Vol. 45, 2011, pp: 1205–1210.

[20] Darwish A., Bayba A.J., Hung, H.A., "*Channel temperature analysis of GaN HEMTs with nonlinear thermal conductivity*", IEEE Transactions on Electron Devices, Vol. 62, 2015, pp: 840-846.

[21] Delagebeaudeuf D., Linh N.T., "*Metal-(n) AlGaAs-GaAs two-dimensional electron gas FET*", IEEE Transactions on Electron Devices, Vol. 29, 1982, pp: 955-960.

[22] Kola, S., Golio, J. M., Maracas, G. N., "*An analytical expression for Fermi level versus sheet carrier concentration for HEMT modeling*", IEEE Electron Device Letters, Vol. 9, 1988, pp: 136-138.

[23] Cadence Design Systems, "*ORCAD PSPICE A/D Reference Manual*", Version 9.2, 2000.

[24] McAndrew C.C., "*Validation of MOSFET model for source/drain symmetry*", IEEE Trans. Electron Devices, Vol. 53, 2006, pp: 2202–2206.

[25] Kumar, S.P., Agrawal, A., Chaujar, R., Kabra, S., Gupta, M., Gupta, R.S., "*Threshold voltage model for small geometry AlGaN/GaN HEMTs based on analytical solution of 3-D Poisson's equation*", Microelectronics Journal, Vol. 38, 2007, pp: 1013-1020.

[26] S. Faramehr, P. Igić and K. Kalna., "*Modelling and optimization of GaN capped HEMTs*", The Tenth International Conference on Advanced Semiconductor Devices and Microsystems, Smolenice, 2014, pp: 1-4.